

A Method for Thermal History Prediction during Additive Manufacturing using Far-Field Temperature Measurements

R. Rangarajan¹, A.E. Segall^{1,*}, R.P. Martukanitz² and F. Lia¹,

¹The Pennsylvania State University

²Materials Science and Engineering, University of Virginia

Abstract: Directed Energy Deposition is a near net-shape, additive manufacturing process that uses high-energy lasers for powder melting and consolidation. While a detailed knowledge of the thermal histories of the process can help understand and ultimately predict the resulting microstructure, residual-stresses, and/or material properties of the component, experimental limitations usually restrict all temperature measurements to far-field locations. When fixed, these measurements become increasingly removed from the laser/material interactions as the build process unfolds. To help offset this limitation, a relatively straightforward method using finite-elements and a fixed far-field measurement was developed that considers experimental processing conditions such as a moving heat source and relevant (and evolving) boundary conditions to generate more complete thermal histories. In essence, an inverse problem was iteratively solved using a direct computational approach. Once validated, the model was then used over multiple depositions with the outcome discussed relative to the agreement and disparities in peak temperatures, heating, and cooling rates. The increasing importance of the growing surface area and evolving radiative and convective boundary conditions with each layer was clearly demonstrated.

Keywords: Additive manufacturing, Lasers, Inverse analysis, Transient temperatures.

1. INTRODUCTION

Additive Manufacturing (AM) is an emerging technology for the fabrication of complex metallic components. Directed Energy Deposition (DED) and Powder Bed Fusion (PBF) are two widely known processes in AM and can deposit a variety of materials on a given substrate. While both processes use lasers with either a Gaussian or a Top-hat profile, the former encompasses an arrangement where the material is fed to the heat source and subsequently deposited. The accurate choice of processing parameters for DED can be challenging, but still very important as it directly impacts the potential creation of process-related defects, microstructure, residual stresses, as well as the eventual material properties of the component. Clearly, the creation of defects and the evolution of microstructure can be better understood by closely observing the thermal history of the process in its entirety. However, direct observations throughout the evolving component are not usually practical so computational approaches are ultimately necessary.

Some of the earlier efforts to understand laser-based manufacturing processes goes back to the work done by Kruth and co-researchers [1] and Bugeda *et al.* [2], where the selective laser sintering process were experimentally and computationally studied based on

both, “performance and feasibility” of CO₂ and Nd:YAG lasers. Following this, a series of computational efforts ensued, including the work of Ghosh and coworkers [3], Roberts and fellow researchers [4], as well as Fischer *et al.* [5]. Ghosh focused on studying the residual stress behavior and resulting microstructures, while Roberts’s study focused on building a robust model to simulate the building process layer-by-layer and simulating its temperature history using an innovative element birth and death technique. Both Ghosh and Roberts concluded that computational models could be used to understand the thermodynamics and mechanical properties of the component during forming.

As more emphasis was placed on simulations, increasingly sophisticated computational models were developed including the work by Michaleris [6]. With goals similar to earlier studies, the newer methodology was based on a combination of element birth and death and inactive element approaches. The work proved that increasingly complex algorithms could be implemented to understand the effects of residual stresses, porosity, laser scan speed, and the resultant microstructures on the properties of the component. Shen and Chou [7] studied such effects by simulating the Electron Beam Additive Manufacturing Process (EBAM) and inspired the studies of Sih and Barlow [8] and Tolochko *et al.* [9] to name a few. The work by Martukanitz and fellow researchers [10] emphasized the importance of accounting for the exact

*Address correspondence to this author at the The Pennsylvania State University, 212 EES Building, University Park, PA 16803; Tel: 814-865-7829; Fax: 814-865-9974; Email: aesevall@psu.edu

environmental conditions, including the moving heat source during fabrication. One of the primary findings was that modeling processes with non-isothermal and actual experimental conditions were key to obtaining realistic results.

While numerical sophistication will yield better predictive results, its high cost and scarce availability will be a limitation. On the other hand, simpler approaches based on limited temperature measurements from a fixed and remote location combined with commercially available FEA tools may prove to be very useful for the refinement and understanding of advanced AM practices. In this work, Directed Energy Deposition was effectively modeled using a 3D mesh and ANSYS along with limited experimental temperatures from a thermocouple at the substrate /deposition interface comprised of Inconel 625. Some key parameters that were shown to impact the process include laser conditions, convective/radiative boundary conditions and the growing surface area, as well as the thermophysical properties of the alloys involved.

2. MATERIALS AND METHODS

2.1. Experimental Setup

All experiments used to obtain data for the guidance and validation of the computational model was conducted at the CIMP-3D facility at the Pennsylvania State University. For these experiments, a 150mm

long, 76mm wide, and 10mm thick Inconel 625 substrate as shown in Figure A1 was used during deposition of five consecutive layers of Inconel 625 of approximately 0.7mm thickness each (*i.e.*, 3.5mm of total deposited material). Temperature dependent Specific Heat, C_p and Thermal Conductivity, k for Inconel 625 are listed in Tables A1 and A2, respectively. The deposition of each layer was across the length of the substrate and confined to the central region as shown in Figure A1. Temperatures as a function of time were measured during all depositions at five different points on the surface of the substrate using tungsten-rhenium thermocouples. The thermocouples were distributed on the top surface at the centerline using a drilled hole from the bottom surface of the plate, with the thermocouple ball being seated at the top surface [11]. Hence, the thermocouple positions would be considered to represent the quasi-steady state condition with respect to the heat source and should display similar thermal responses. This enabled the various thermocouple responses to be used as replications of the measured data. Figure A2 depicts the side view of Figure A1 and the placement of the five thermocouples on the surface of the substrate. The Inconel 625 substrate was placed 80mm over an aluminum plate using four steel rods supported at the four corners to enable convection and radiation on all surfaces. As mentioned earlier, all layers were deposited using the DED process. Argon was always used as the shielding gas with a flow rate of 20 ft³/hr (9.44 L/min).

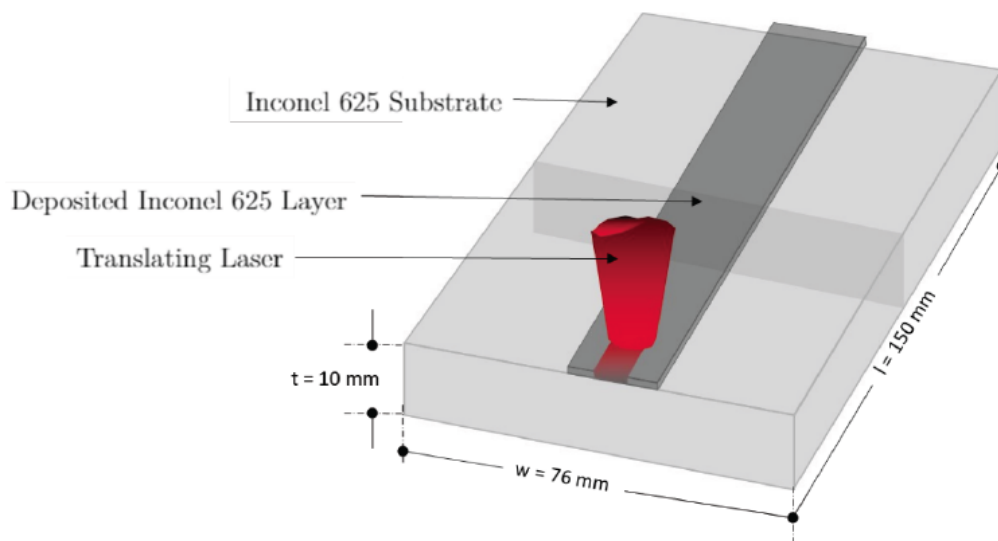


Figure A1: 3D rendering of the experimental DED Setup with an Inconel 625 substrate over which multiple layers of Inconel 625 were deposited.

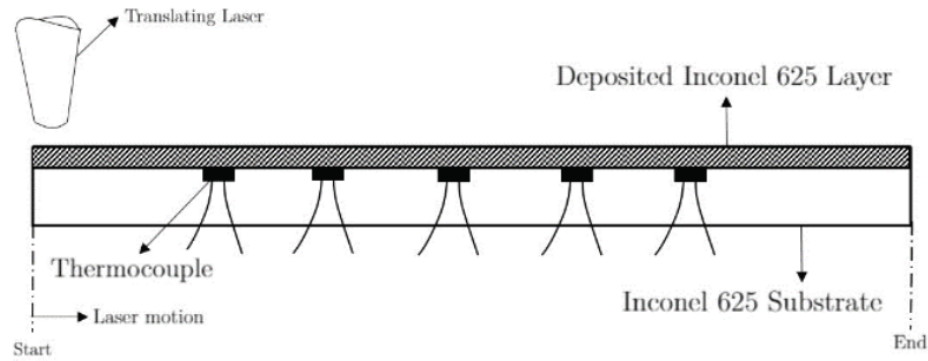


Figure A2: Experimental DED of an Inconel 625 substrate showing the thermocouple positioning.

Table A1: Temperature Dependent Specific Heat Capacity of Inconel 625

Specific Heat (J/kg- °C)	Temperature (°C)
410	21
427	93
456	204
481	316
511	427
536	538
565	649
590	760
620	871
645	982
673	1100
685	1150
697	1200
709	1250

2.28E-02	871
2.52E-02	982
2.53E-02	1000
2.62E-02	1050
2.72E-02	1100
2.81E-02	1150
2.91E-02	1200
3.01E-02	1250

During all depositions, a high power Yb:YAG laser with a Precitec YW50 head at a 212mm standoff was used; laser scan speed was 10.58 mm/s with a power of 2000 W. Deposition of each layer required approximately 20s with the data recorded at an acquisition rate of 60 Hz. At the end of each 20s deposition cycle, the laser was repositioned to its starting point to begin the process for the next layer as articulated for three steps in Figure A3. As already mentioned, the final fifth-layer build was approximately 3.5mm thick, 4.4mm wide, and 150mm in length.

Table A2: Temperature Dependent Thermal Conductivity of Inconel 625

Thermal Conductivity (W/mm-°C)	Temperature (°C)
9.20E-03	-18
9.80E-03	21
1.01E-02	38
1.08E-02	93
1.25E-02	204
1.41E-02	316
1.57E-02	427
1.75E-02	538
1.90E-02	649
2.08E-02	760

2.2. Simulations

The experimental conditions and initial substrate/deposition interface discussed above were used in concert with the ANSYS finite-element code to develop a computational model of the process; As discussed in detail below, the complex fabrication process and any reasonable simulations of it demanded a meticulous understanding of the environment and any stray heat transfer to the surrounding environment.

Convection and Radiation

Considering the fact that each layer was only 0.7mm thick, radiation and convection from the sides of the first three layers (i.e. 2.1mm total wall height) were

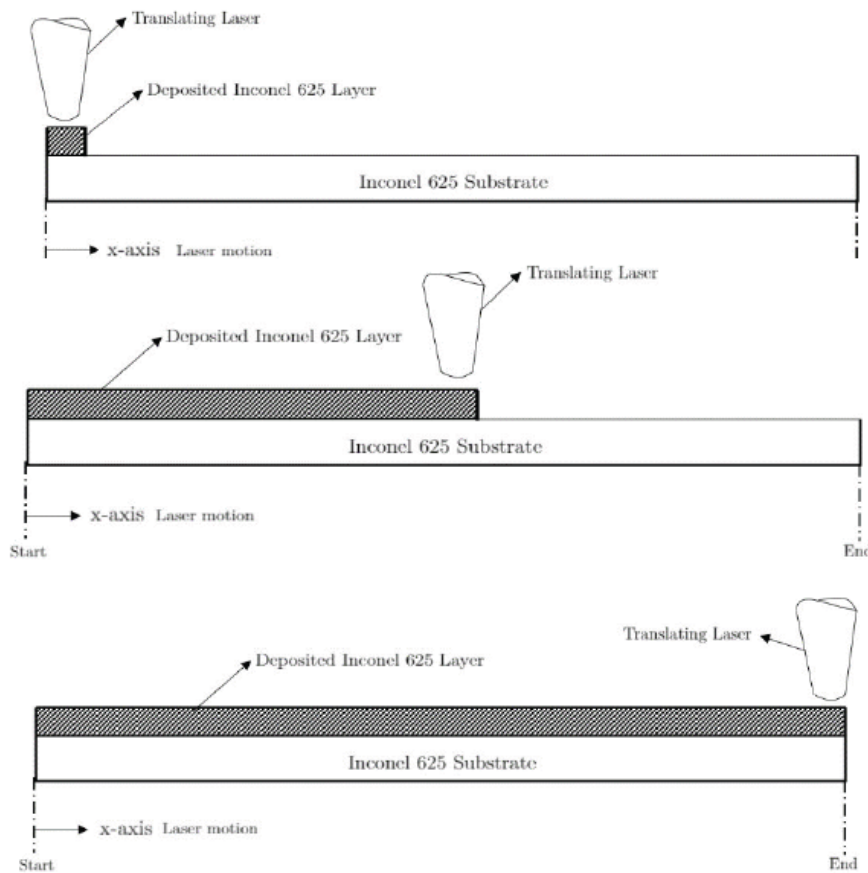


Figure A3: Laser position at $t = 0s$ and $x = 0$ (top), $t = 10$ seconds and $x = 75mm$ (middle), and $t = 20$ seconds and $x = 150mm$ (bottom).

assumed to be relatively small. Nonetheless, the effect of energy absorption by these layers does still potentially impact the thermal history of the fourth and fifth layer. The sides of the previously deposited layers radiate and convect heat, and it is essential to model them as boundary conditions.

Values were ultimately estimated for different portions of the geometry based on the research conducted by Heigel *et al.* [12] and Gouge and coworkers [13] that was in-part, predicated on earlier work [14]. Based on this guidance for a gas flow rate of 9.44 liters per second, the forced convection coefficient was estimated to be between $40W/m^2/K$ - $107W/m^2/K$. Similarly, the average forced convection coefficient was $65W/m^2/K$ with the free surface convection $9W/m^2/K$, and an emissivity of 0.40.

Symmetry

By design, the geometry of the deposited layers and substrate exhibited symmetry so that all temperature measurements would not be influenced by uneven heat transfer via conduction, convection, and/or thermal

radiation. Such symmetry, allowed for a significantly smaller FEA mesh with all borders treated as adiabatic, thus saving considerable computational time. Figure A4 depicts the mesh for the geometry with the substrate (top) and a single deposited layer (bottom); in its entirety and comprising all five layers of the build, the mesh consisted of 165,000 elements and 176,052 nodes. The primary region of interest for the simulations was on the surface of the substrate (first layer/substrate interface), similar to experimental setup.

Moving Heat Source

A high power Yb:YAG laser was used to melt and deposit multiple layers of Inconel 625 onto a substrate made from the same material. In order to build a realistic computational model, the laser was simulated as a moving boundary flux denoted as Q ; an intensity equation as a Gaussian function representing the absorbed laser energy was derived and is shown as:

$$Q = \frac{2\beta P}{\pi s^2} e^{-2r} \quad (1)$$

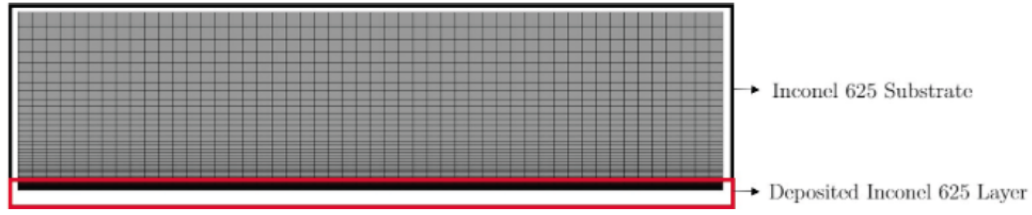


Figure A4: Top-view of the meshed geometry. The deposited layers are blacked out due to the fine mesh while the coarse mesh for other areas are depicted.

where

$$r = \left[\frac{(x_c - x_{st} - vt)^2 + (y_c)^2}{s^2} \right]^N \quad (2)$$

and β is the bulk absorption coefficient, P represents power, s is the laser spot radius, r denotes the super-Gaussian distribution function for the moving heat source, x_c is the position of the laser on the x-axis, x_{st} indicates the starting position of the laser, v is the laser velocity, t is time, y_c is the position of the laser on the y-axis, and N is the super-Gaussian factor for a top-hat distribution. For the current tests and simulations, the velocity of the laser was set at 10.58 mm/s and the flowtime was 20 seconds. Additionally, the power of the laser was designated to be 2000W with an approximated bulk absorption coefficient of 0.4 and a spot radius of 3mm [15]. Various laser parameters used in the study are listed in Table A3.

Table A3: Laser Parameters

Absorption Factor	0.4
Scan Speed	10.58 mm/s
Power	2000 W
Layer Thickness	0.7mm per layer

Numerical Setup

The numerical method employed in this analysis enforces the energy conservation law to a control volume (CV) with relevant boundary conditions at each node in a given mesh. The underlying principle used was the Fourier law with appropriate boundary conditions applied:

$$\rho C_p \frac{\partial T}{\partial t} = \nabla \cdot (k \nabla T) \quad (3)$$

The basic energy balance formulation as given by Equation 4 below, represents the change in internal energy (U) from the heat entering and leaving the CV

($q_{\text{conduction}}$), convection ($q_{\text{convection}}$) and radiation ($q_{\text{radiation}}$) losses at the surfaces, and the heat flux from the laser (Q).

$$U = q_{\text{conducted}} - q_{\text{convected}} - q_{\text{radiated}} + Q \quad (4)$$

Figure A5 shows a control volume analysis that provide the basis for the solution in its entirety. From this analysis, the final form of the energy balance equation, in three dimensions can be represented as:

$$Q_{\text{laser}} = h(T_{i,j} - T_{\infty}) + \epsilon \sigma (T_{i,j}^4 - T_{\infty}^4) - k \left(\frac{\partial^2 T_{i,j}}{\partial x^2} + \frac{\partial^2 T_{i,j}}{\partial y^2} + \frac{\partial^2 T_{i,j}}{\partial z^2} \right) + \rho C_p \frac{dT_{i,j}}{dt} \quad (5)$$

where h is the convection coefficient, ϵ represents the emissivity, $T_{i,j}$ is the temperature at the node on the i^{th} row and j^{th} column, k denotes the thermal conductivity, σ is the Stefan-Boltzmann constant ($5.67E-8 \text{ W.m}^{-2}.\text{K}^{-4}$), ΔT represents the change in temperature across the control volume, Δz the thickness of the control volume, and T_{∞} is the atmospheric or far-field temperature.

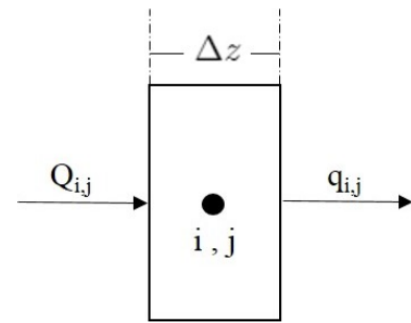


Figure A5: Control Volume Analysis using the discussed method on the i^{th} row and j^{th} column, where $q_{i,j}$ is the summation of losses due to convection, radiation and conduction and $Q_{i,j}$ is the heat flux from the laser.

Implementation per Layer

For each layer under construction, the laser translates and then repositions itself before the next pass begins. After each pass, a portion of the heat absorbed in the newly deposited and existing layers

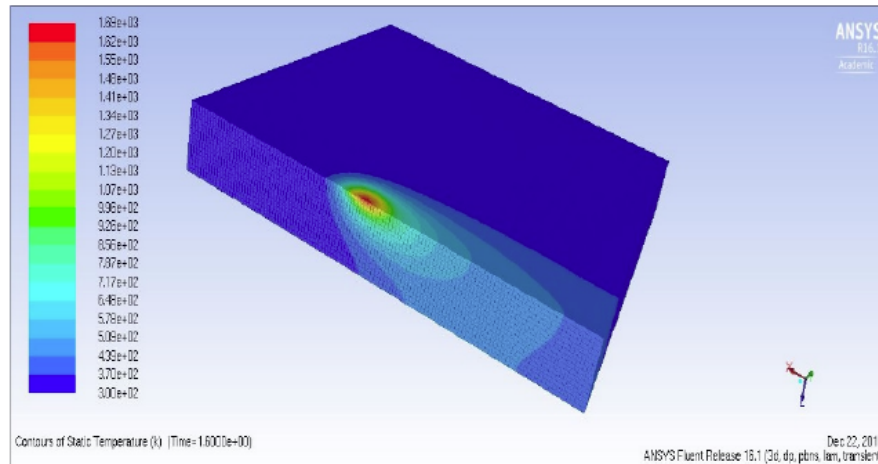


Figure A6: Illustration of the moving heat source in real time used to deposit Inconel 625 over the substrate.

are sufficient to increase their temperatures. This implies that the next layer of powder to be deposited is initially at a much lower temperature, thus dictating the need for temperature initialization.

A user defined function (UDF) was employed within ANSYS and designed to control the laser location from start to finish on the top face over the layer that was being deposited. Each pass lasted for approximately twenty seconds, after which the final temperature was recorded and used for initialization for the next layer. The convergence criteria monitored temperature residuals at each control volume using the above derived questions at an absolute criterion of 0.001. The temperature contours and highly localized nature of the high temperature region seen in Figure A6 indicate the near instantaneous effect of the laser. The results obtained from the model for the deposition of the first layer was then used for validation purposes against the experimental data. The experimental data from the thermocouples were averaged into a single temperature value for each time-step (Figure A2).

3. RESULTS AND DISCUSSION

The temperatures for each layer deposition was recorded in addition to the overall thermal history of the evolving structure. Figure A7 compares the experimental data with the simulations for all the layers. As anticipated, the convective and radiative boundary conditions primarily impacted layers 4 and 5 as the available (side) surface area increased. A breakdown of the individual layer formation is discuss below, while Table A4 shows a summary of the obtained results for all five layers.

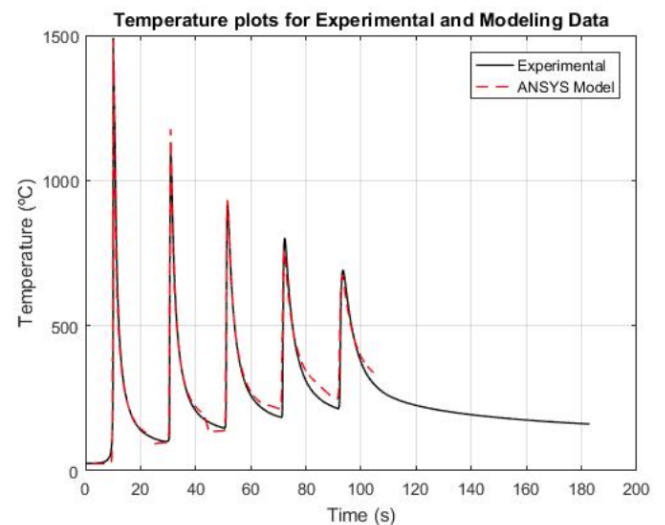


Figure A7: Experimental Data and Model Prediction of the five deposited layers.

First Layer Deposition

Result obtained for a deposition time of approximately 20s gave a peak temperature of 1482 °C as compared to the original data with a value of 1491 °C. Additionally, the rate of cooling is also in relatively good agreement with the experimental data in terms of magnitude and trends. However, there is a subtle disparity in the rate of heating and cooling between the two data sets, which can be attributed to the fact that the experimental data is the average temperature from five thermocouples at the various locations on the surface of the substrate. Moreover, the disparity may stem from the lack of intimate contact between the thermocouples and the surrounding substrate prior to melting by the laser. As additional layers are deposited, such effects would become less significant as the

Table A4: Peak Temperature Tabulation after the Deposition of each Layer

Layer	Experimental Peak Temperature (°C)	Standard Deviation Experimental Data	Model Prediction (°C)	Standard Deviation Model Data	Percent Difference (%)
1	1491	306.63	1482	256.86	0.60
2	1105	238.09	1177	237.35	6.52
3	915	200.15	932	210.37	1.86
4	800	164.28	759	147.45	5.13
5	690	121.19	671	115.45	2.75

greater thermal mass and distance along with the growing attenuation of laser heating would tend to dampen the thermal response.

Second Layer Deposition

As additional layers were formed over the substrate and previous depositions, the distance and accompanying lag (impedance) between the thermocouple and build increases, as just discussed. Moreover, the overall temperatures of the evolving system have increased in both magnitude and complexity (gradients with increasing thickness) due to uneven conduction to the substrate, as well as non-uniform convection and radiation to the environment. Simulation results for the second layer provides a peak temperature of 1177 °C as compared to the measured values of 1105 °C; the error in the peak values was ~6.52% and the disparity can be attributed to the factors mentioned in the previous section. In hindsight, it is likely that the surfaces of the first two layers and/or the substrate may have drawn more heat to the environment than originally thought due to the latent heat present in the system from the previous layer. Nonetheless, the overall heating and especially the cooling trends as seen by the curves in Figure A7 show very good agreement.

Third Layer Deposition

As the third layer was deposited, the overall component thickness increased by 2.1mm so that the convective and radiative surfaces were becoming increasingly important and required an initialization of the boundary conditions. Specifying a surface convection with a coefficient of 40 W/m²/K on the entire geometry, the obtained results show a peak temperature of 932°C as compared to 915°C. In this case, the error was 1.86% and most of the cooling rate at different time-steps were in good agreement, albeit slightly slower. Figure A8 shows a magnified

comparison of the measured and predicted thermal history during the deposition of the 3rd layer.

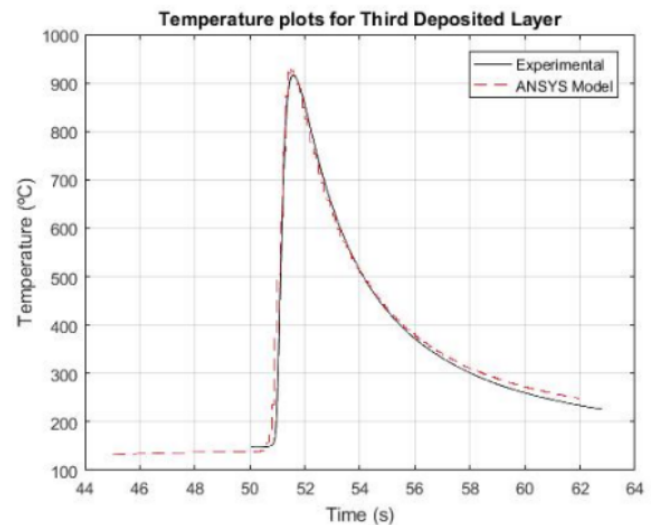


Figure A8: Thermal History after the deposition of the third layer.

Fourth and Fifth Layer Depositions

The effects of the various boundary conditions and temperature initialization had an impact on layers 4 and 5, as they influenced the rate of heating and cooling. The initial setup was simulated with the same convection coefficient for layer 3, but did not account for any radiation, which resulted in significant disparities in the cooling rate. Figure A9 illustrates the thermal history without radiation from the walls. Although the rate of heating was in agreement with experimental data, cooling was higher than expected with a maximum error of 14% in the fourth layer and 10% in the fifth layer. To improve performance, an emissivity of 0.3 was applied on the sides on the previously deposited layers and the convection coefficient was increased to 65 W/m²/K. As also shown in Figure A9, the experimental rate of cooling was still faster with a maximum error of 9.86% in the fourth layer and 6.81% in the fifth layer.

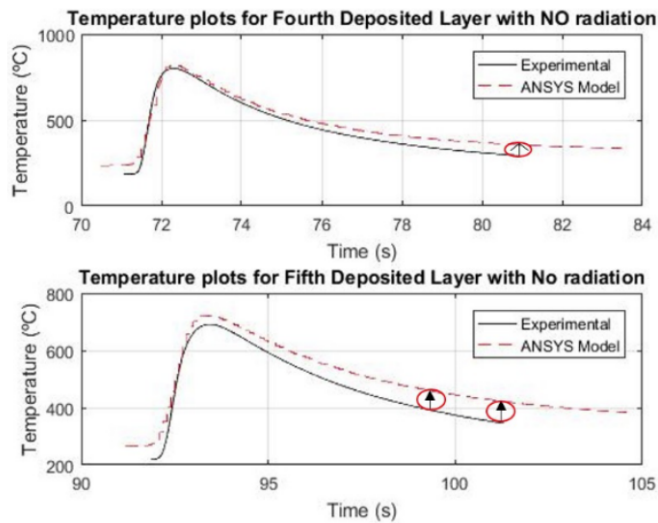


Figure A9: Thermal History after the deposition of the fourth and fifth layer without radiation on the sides of the wall. The differences in the rate of cooling is highlighted and circled.

Additionally, the peak temperatures for the fifth layer were in agreement when compared to the result without radiation. Further study on the thermal history was performed by increasing the emissivity to from 0.3 to 0.4, following the work done by Gouge *et al.* [13]. Figures A10 and A11 depict the thermal histories for both values. Overall, the rate of cooling error using emissivity values of 0.3 and 0.4 did not seem to affect the fourth layer, while the error seen for the fifth layer dropped by 1.73% (6.81% to 5.08%); the differences in the cooling rates are circled in Figure A10. The Inconel 625 substrate was placed above an aluminum plate so it is likely that the bottom of the substrate was also radiating heat out of the system at an increasing rate as the heat in the system increased. In addition to having the walls radiate energy with an increased emissivity of 0.4, the model was refined by factoring in the radiation to the aluminum with an estimated emissivity of 0.2. For all subsequent simulations, a forced convection coefficient of $65 \text{ W/m}^2/\text{K}$ was used on the bottom surface of the substrate, while the sides utilized values of $10 \text{ W/m}^2/\text{K}$.

For the given set of boundary conditions and initial conditions, the peak temperatures from the model for the fourth layer was relatively close at 759°C as compared to the experimentally determined value of 800°C , or a difference of 5.13%. On the other hand, the predicted fifth layer temperature was 671°C or 2.75% lower than the experimentally determined 690°C . The error in the cooling rate for the fourth layer was roughly 9% and the fifth layer was 5.08%. Although the model improvement was iterative, the inference from the

effects of radiation and convection at each level were instrumental in fine tuning the applied boundary conditions to match the data. Nonetheless, the method was able to reasonably approximate the deposition process without numerous changes to the model parameter. Hence, limited and remote temperature measurements could be effectively used with a standard finite-element model to determine thermal profiles of a multi-layer AM build under very complex thermal conditions.

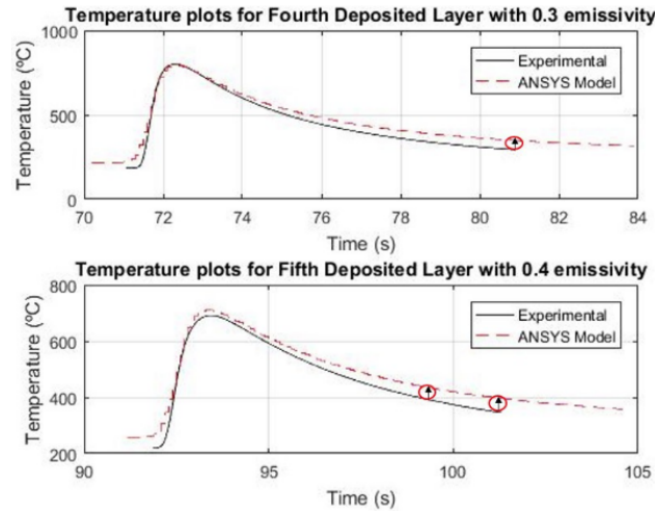


Figure A10: Thermal History after the deposition of the fourth and fifth layer with 0.3 emissivity on the sides of the wall. The differences in the rate of cooling is highlighted and circled.

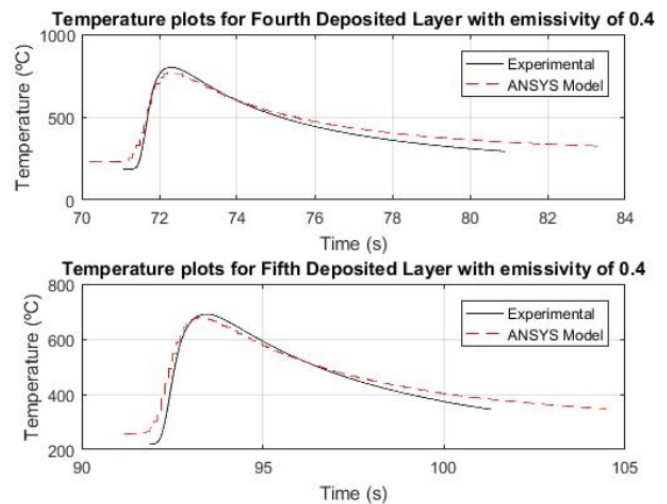


Figure A11: Thermal History after the deposition of the fourth and fifth layer with 0.4 emissivity on the sides of the wall.

The step-by-step improvement seen for layers four and five show the importance of accounting for changes in convection and radiation boundary conditions. As clearly shown by the results, the growing number of layers, the increased heat in the system

(build and substrate), and associated stray heat transfer to the environment does indeed impact the peak temperatures and the rate of cooling between laser passes. While the heat buildup and changing boundary conditions will also influence the heating rate, the net effect is much smaller due to the dominance of the energy coming from the laser. All the boundary conditions used in the simulation were based on the environment in which the experiments were performed and can be altered accordingly. Another area for further refinement should include an initialization function which considers an imposed temperature gradient in the new layer before additional deposition.

The analysis has demonstrated the capacity to approximate a very complex event based on known and/or assumed boundary conditions, limited temperature measurements, and a Direct approach using commercially available finite-element codes. While the matching of the measure temperatures was ultimately very good, the Inverse method must be considered approximate at best because it is inherently ill posed and therefore sensitive to errors in the data. Moreover, it is simulating a complex event with distinct nonlinearities given the known temperature dependencies of the thermophysical properties and phase changes in the melting/solidifying layer. While both nonlinearities can be handled using FEA, only the temperature dependencies of the properties were considered for the current analysis since the phase changes are occurring over a relatively thin layer and the temperature should be highly dependent upon the incoming energy from the laser, especially as more layers are added and the temperature measurement is increasingly remote; the accuracy of the analysis and ensuing temperature gradients is most likely best in the solid portions of the build and less accurate in the top layer under the incoming laser energy. Given that the back-side boundary conditions are relatively straightforward (convection and radiation to the surrounding environment), the overall estimation of the thermal state and gradients throughout should be highly reflective of an AM build even based on limited temperature measurements.

While approximate at best, the method does not require specialized codes and is capable of identifying the temporal variations of temperature as the build ensues. This valuable information can be used to improve the build process by identifying regions where the temperature distributions are changing rapidly or are somewhat static. For instance, the simulation can be used to identify hot and/or cool regions that may be

problematic with regards to the development of residual stresses, which could indicate potential distortion or cracking. Additionally, slower cooling regions may see changes and/or unwanted growth in the microstructure that could render various properties (strength, elastic modulus, etc.) inferior to the rest of the build.

4. CONCLUSION

Based on the results obtained for each deposited layer, the key conclusions are as follows:

The analysis and Direct finite-element thermal simulations described above have demonstrated the ability to estimate a very complex event involving laser induced phase changes based on limited and remote temperature data along with known/assumed boundary conditions.

As intended, the simulations for the first layer was guided and validated based on the experimental data measured using averaged data from thermocouples positioned on the substrate surface. Initially, the percent error between measured and predicted temperatures ranged from 0.6-8% depending on the Super-Gaussian factor employed, speed of translation, and boundary conditions governing the stray heat transfer to the environment. After refining the boundary conditions, peak values and overall heating and cooling curves better correlated with the measured data and consecutive layers were simulated with relative errors ranging from 2-5%. The relatively good agreement between values and the temperature-time relationships during both heating and cooling, implies the model can reasonably represent the process for deposition of multiple layers using standard FEA approaches.

As the number of layers and overall heat of the system increased, the effects of both radiation and convection from the top, sides, and bottom of the substrate become progressively important; this is due to the creation of additional surface area representing the blade that increases convective and radiative cooling, as well as the increasing temperatures of the build and substrate.

It should be noted that the overall goal of the research was to simulate the thermal history in a time effective method and to study its sensitivity to the evolving heat build-up and stray heat transfer conditions. As anticipated, the results showed that limited and remote temperature measurements could be effectively used to guide the modeling of an AM build under very complex thermal conditions using a

non-specialized FEA formulation, provided the evolving boundary conditions were considered. The results of such simulations can be used to identify thermal regions that may be problematic with regards to the development of residual stresses, unwanted growth in the microstructure, property variations, as well as the potential for distortions that could all lessen the overall quality of the AM build.

REFERENCES

- [1] Kruth JP, Peeters P, and Smolderen T. Comparison between CO₂ and Nd:YAG lasers for use with selective laser sintering of steel-copper powders, *Journal of CAD/CAM Computer Graphics* 1998; 13(4-6).
- [2] Bugada G and Lombera G. Numerical prediction of temperature and density distributions in selective laser sintering processes, *Rapid Prototyping Journal* 1999; 5. <https://doi.org/10.1108/13552549910251846>
- [3] Ghosh S and Choi J. Three-dimensional transient finite element analysis for residual stresses in the laser aided direct metal/material deposition process, *Journal of Laser Applications* 2004; 17(3). <https://doi.org/10.1115/HT-FED2004-56359>
- [4] Roberts I, Wang CJ, Esterlein R, Stanford M and Mynors, DJ. A three-dimensional finite element analysis of the temperature field during laser melting of metal powders in additive layer manufacturing, *Elsevier* 2009; 49: 916-923. <https://doi.org/10.1016/j.ijmachtools.2009.07.004>
- [5] Fisher P, Romano V, Weber HP, Karapatis NP, Boillat E and Glardon R. Sintering of commercially pure titanium powder with a Nd:YAG laser source, *Acta Materialia* 2003; 51: 1651-1662. [https://doi.org/10.1016/S1359-6454\(02\)00567-0](https://doi.org/10.1016/S1359-6454(02)00567-0)
- [6] Michaleris P. Modeling metal deposition in heat transfer analyses of additive manufacturing processes 2014; 86: 51-60. <https://doi.org/10.1016/j.finem.2014.04.003>
- [7] Shen N and Chou K. Thermal modeling of electron beam additive manufacturing process - powder sintering effects 2012. <https://doi.org/10.1115/MSEC2012-7253>
- [8] Sih S and Barlow J. The prediction of the emissivity and thermal conductivity of powder beds, *Particulate Science and Technology* 2004; 22: 291-304. <https://doi.org/10.1080/02726350490501682a>
- [9] Tolochko N, Arshinov MK, Gusarov AV, Titov VI, Laoui T, and Froyen L. Mechanisms of selective laser sintering and heat transfer in Ti powder, *Rapid Prototyping Journal* 2003; 9: 314-326. <https://doi.org/10.1108/13552540310502211>
- [10] Martukanitz R, Michaleris P, Palmer T, DebRoy T, Liu Z, Otis R, Heo TW and Chen L. Toward an integrated computational system for describing the additive manufacturing process for metallic materials, *Elsevier* 2014; 1-4: 52-63. <https://doi.org/10.1016/j.addma.2014.09.002>
- [11] Lia F, Park JZ, Keist JS, Joshi S, Martukanitz RP. Thermal and microstructural analysis of laser-based directed energy deposition for Ti-6Al-4V and Inconel 625 deposits, *Penn State Materials Science & Engineering* 2018; A: 717, pp. 1 <https://doi.org/10.1016/j.msea.2018.01.060>
- [12] Heigel J, Michaleris P and Palmer T. Measurement of forced surface convection in directed energy deposition additive manufacturing, *Journal of Engineering Manufacture* 2015; 230(7). <https://doi.org/10.1177/0954405415599928>
- [13] Gouge M, Heigel JC, Michaleris P and Palmer TA. Modeling forced convection in the thermal simulation of laser cladding processes, *The International Journal of Advanced Manufacturing Technology* 2015; 79(1). <https://doi.org/10.1007/s00170-015-6831-x>
- [14] Non-contact temperature measurement, *Technical Report Transactions* 1998; 1.
- [15] Lia F, Park J, Tressler J and Martukanitz R. Partitioning of laser energy during directed energy deposition, *Additive Manufacturing* 2017; 18: 31-39 <https://doi.org/10.1016/j.addma.2017.08.012>

Received on 20-7-2019

Accepted on 7-8-2019

Published on 30-8-2019

DOI: <http://dx.doi.org/10.31875/2409-9848.2019.06.4>

© 2019 Rangarajan *et al.*; Zeal Press.

This is an open access article licensed under the terms of the Creative Commons Attribution Non-Commercial License (<http://creativecommons.org/licenses/by-nc/3.0/>), which permits unrestricted, non-commercial use, distribution and reproduction in any medium, provided the work is properly cited.